

# Ionized gas rotation curves in nearby dwarf galaxies

A. V. Moiseev

Special Astrophysical Observatory, Russian Academy of Sciences<sup>\*</sup>, Nizhnij Arkhyz, 369167, Russia

September 10, 2013/Revised October 4, 2013

**Abstract.** We present the results of study of the ionized gas velocity fields in 28 nearby (systemic velocity below  $1000 \text{ km s}^{-1}$ ) dwarf galaxies. The observations were made at the 6-m BTA telescope of the SAO RAS with the scanning Fabry–Perot interferometer in the  $H\alpha$  emission line. We were able to measure regular circular rotation parameters in 25 galaxies. As a rule, rotation velocities measured in HII are in a good agreement with the data on the HI kinematics at the same radii. Three galaxies reveal position angles of the kinematic axis in the HII velocity fields that strongly (tens of degrees) differ from the measurements in neutral hydrogen at large distances from the center or from the orientation of the major axis of optical isophotes. The planes of the gaseous and stellar disks in these galaxies most likely do not coincide. Namely, in DDO 99 the gaseous disk is warped beyond the optical radius, and in UGC 3672 and UGC 8508 the inclination of orbits of gas clouds varies in the inner regions of galaxies. It is possible that the entire ionized gas in UGC 8508 rotates in the plane polar to the stellar disk.

## 1. INTRODUCTION

Rotation curve is one of the main characteristics of galaxies, accessible to direct measurements. Knowing the radial distribution of rotation velocity, we can, given certain approximations, estimate the distribution of mass, including that of dark matter. It is rather difficult to measure the rotation curve of gas in dwarf galaxies. This is due to their small mass, and hence the velocity of regular rotation is only a few tens of  $\text{km s}^{-1}$  which is comparable to the amplitude of noncircular gas motions related to the regions of current star formation. It is often not enough here to only have to cross-section the line of sight velocity distribution along the major axis of the disk, but we additionally need to analyze the two-dimensional distribution of line of sight velocities (the velocity field) to be able to fit it using the model of circular rotation.

Therefore, most of the reliable rotation curves of gas in dwarf galaxies published are obtained from the HI observations in the 21 cm line, applying the aperture synthesis method. However, even using sufficiently large databases, the angular resolution of these observations is not very large, e.g., amounting to  $13\text{--}61''$  in the FIGGS survey (Begum et al., 2008). Recent observations for the LITTLE THINGS sample (Hunter et al., 2012) were obtained with a resolution of  $6\text{--}10''$ , which can be considered record high in this kind of studies. However, many scientific problems require the knowledge of gas kinematics with a better spatial resolution. For instance, this is the

case with the study of the central regions of dwarf galaxies, where the divergence of the actual rotation curve from the predictions of numerical calculations is the most conspicuous (the nuclear cusp problem, see, e.g., the review by Doroshkevich et al., 2012).

The observations with the scanning Fabry–Perot interferometer (FPI) in the ionized gas emission lines allow to construct radial velocity fields with the seeing-limited angular resolution (usually  $1\text{--}2''$ ). However, the disadvantage of the HII line measurements, as compared with HI, is a smaller filling of the velocity field, since the emission in the Balmer lines is visible only where there is a sufficient number of UV photons, the main source of which are young, massive stars. In order to detect diffuse gas emission away from the regions of star formation, large optical telescopes or hours of scanning cycles at the instruments of small diameters are required. Therefore, most of the observations of dwarf galaxies with the IFP were carried out for the objects with a relatively strong star formation, such as the blue compact galaxies (Ostlin et al., 1999; Lozinskaya et al., 2006). About two dozen dIrr galaxies were also observed within the GHASP survey (Epinat et al., 2008), but an insufficient limit of these observations has often not allowed to build the rotation curves in the galaxies deprived of bright HII regions.

In this regard, combining the rotation curves obtained for the central regions of galaxies from the ionized gas data with the results from neutral hydrogen data for the more external regions appears to be promising. This paper is one of the steps in this direction. We present here the reduction results of the archival observations

Send offprint requests to: A. Moiseev e-mail: [moisav@sao.ru](mailto:moisav@sao.ru)

<sup>\*</sup> The system of Russian Academy of Sciences institutes was liquidated (“re-organized”) on Sep 2013

of nearby dwarf galaxies (systemic velocity of less than  $1000 \text{ km s}^{-1}$ ), performed with a scanning FPI on the 6-m BTA telescope of the Special Astrophysical Observatory of the Russian Academy of Sciences. Most of the studied objects were observed within the proposal of A. A. Klypin, and the rest of them—on the requests of A. Begum, T. A. Lozinskaya, and S. A. Pustilnik. Further, Section 2 describes the observations and data reduction, Section 3 discusses the technique of construction of rotation curves, Section 4 presents our results (velocity fields and rotation curves), and finally, Section 5 gives comments on the kinematic features of individual galaxies.

## 2. OBSERVATIONS AND DATA REDUCTION

The observations were conducted in the primary focus of the 6-m BTA telescope of the SAO RAS with the scanning FPI installed inside the SCORPIO focal reducer (Afanasiev & Moiseev, 2005). The operating spectral range around the  $H\alpha$  line was cut by the narrow-band filters with a bandwidth of  $\text{FWHM} = 14\text{--}21 \text{ \AA}$ . Until November 2009 the observations were made with the IFP 501 interferometer providing in the  $H\alpha$  line a free spectral range between the adjacent interference orders of  $\Delta\lambda = 13 \text{ \AA}$  and spectral resolution (FWHM of the instrumental profile) of about  $0.8 \text{ \AA}$  ( $35 \text{ km s}^{-1}$ ) at the scale of  $0.36 \text{ \AA}$  per channel. Later we used the IFP 751 interferometer having  $\Delta\lambda = 8.7 \text{ \AA}$  and spectral resolution of  $0.4 \text{ \AA}$  ( $18 \text{ km s}^{-1}$ ) at the scale of  $0.21 \text{ \AA}$  per channel.

The detectors used in 2005–2010 were the EEV 42-40 and E2V 42-90 CCDs, providing the image scale of  $0''.71 \text{ pixel}^{-1}$  in the  $4 \times 4$  binning readout mode. In 2002 the TK 1024 CCD was used as a detector, providing the image scale of  $0''.56 \text{ pixel}^{-1}$  in the  $2 \times 2$  binning mode.

In the scanning process we have consistently obtained the object interferograms (36 for IFP 501 and 40 for IFP 751) at different distances between the IFP plates. Reduction of the observational material was performed using the software package operating in the IDL environment (Moiseev, 2002; Moiseev & Egorov, 2008). The reduction result is a data cube where each pixel in the field of view contains a 36- or 40-channel spectrum.

The log of observations is given in Table 1 containing: the name of the galaxy (adopted in the paper and the alternative, if it is commonly used), the date of observations, the interferometer name, exposure time, image quality (seeing), and final angular resolution ( $\omega$ ) after smoothing the reduced data cubes by a two-dimensional Gaussian to increase the signal-to-noise ratio in the regions of low surface brightness.

The observed  $H\alpha$  line profiles were approximated by the Voigt function, which describes them well enough in most of cases. According to the results of profile approximations, we have built the ionized gas line of sight velocity fields and line of sight velocity dispersion maps as well as the images of galaxies in the  $H\alpha$  emission line and in the continuum. Some of these maps for seven galaxies of

our list have already been presented in our previous paper (Moiseev & Lozinskaya, 2012), where we discuss the features of distribution of the ionized gas velocity dispersion.

## 3. KINEMATICS ANALYSIS

### 3.1. Moderately Inclined Disks

The inclination of the disk plane to the line of sight  $i_0$  does not exceed  $70^\circ$  for most of the galaxies considered. We can neglect the thickness of the gaseous disk here and approximate the observed velocity fields within the commonly used tilted-rings approximation. We used the software package, written in the IDL, implementing the adaptation of this method for the ionized gas velocity fields (Moiseev et al., 2004; Moiseev, 2008, *ibid* references to earlier studies)).

During the analysis, the observed velocity field is split into  $1\text{--}5''$ -wide elliptical rings in agreement with the adopted inclination  $i_0$  and position angle of the major axis of the disk  $PA_0$ . In each ring, we fit the observed distribution of line of sight velocities by the circular rotation model, using the  $\chi^2$ -minimization. Model parameters are the position angle of the kinematic major axis  $PA_{\text{kin}}$ , the inclination of circular orbits  $i$ , circular rotation velocity  $V_{\text{rot}}$ , and systemic velocity  $V_{\text{sys}}$ . If one can be sure that the disk plane has no large warps, we can accept the inclination and systemic velocity to be radius-independent ( $i(r) = i_0$ ,  $V_{\text{sys}}(r) = \text{const}$ ). In this case, radial variations of  $PA_{\text{kin}}$  reflect the behavior of non-circular components of the three-dimensional velocity vector of gas clouds, for example, as a result of disturbance by the spiral density waves.

Expanding shells, induced by star formation in dwarf galaxies, can significantly distort the velocity field of the disk, since the amplitude of the rotation curve is small and comparable to the shell expansion velocity ( $10\text{--}30 \text{ km s}^{-1}$ ), while the size of the shell may be comparable to the size of the disk. We have shown in Moiseev et al. (2010b) that in this case it is necessary to fix the  $V_{\text{sys}}$ ,  $i$  and  $PA_{\text{kin}}$  parameters to avoid systematic errors in the measurement of rotation velocities by the tilted-rings method.

This is why the analysis of the velocity fields is carried out as follows. As the first approximation for  $PA_0$ ,  $i_0$  and the center of rotation, we have adopted the existing orientation parameters according to the photometry data<sup>1</sup> or HI maps. Their further refinement is done by successive approximations, while at each step we masked the regions notable for their peculiar kinematics, i.e., deviating by more than  $6\text{--}10 \text{ km s}^{-1}$  from the model of circular rotation (this threshold was individually selected). If the center of symmetry of a velocity field lies no further than  $1\text{--}3''$  from

<sup>1</sup> If the authors listed the ellipticity isophotes only, the corresponding  $i_0$  were calculated according to the relation Staveley-Smith et al. (1992) for dwarf galaxies.

normal

**Table 1.** Log of observations

Name	Alt. name	Date	FPI	Exp. time, sec	Seeing, arcsec	$\omega$ , arcsec
CGCG 269-049	[KK 98] 149	Feb 06, 2010	IFP 751	$150 \times 40$	3.5–4.4	4.4
DDO 53		Feb 26, 2009	IFP 501	$200 \times 36$	2.3–2.5	3.3
DDO 68		Dec 30, 2006	IFP 501	$240 \times 36$	1.5–2.7	2.7
DDO 99		Feb 26, 2009	IFP 501	$180 \times 36$	2.0–3.0	3.8
DDO 125		May 18, 2005	IFP 501	$180 \times 36$	1.5–1.8	3.0
DDO 190		Mar 04, 2009	IFP 501	$100 \times 36$	2.2–2.5	3.3
KK 149		Mar 05, 2009	IFP 501	$150 \times 36$	1.9–2.5	2.8
KKH 12		Aug 23, 2004	IFP 501	$120 \times 36$	1.8–2.0	2.7
KKH 34		Nov 12, 2009	IFP 751	$230 \times 40$	1.9–3.1	3.4
KKR 56		May 20, 2010	IFP 751	$150 \times 40$	2.5–3.0	3.3
UGC 231	NGC 100	Nov 11, 2009	IFP 751	$200 \times 40$	1.4–2.3	2.4
UGC 891		Nov 11, 2009	IFP 751	$200 \times 40$	2.0–3.1	3.1
UGC 1281	NGC 784	Aug 14, 2009	IFP 751	$110 \times 40$	1.5–1.7	2.7
UGC 1501		Nov 10, 2009	IFP 751	$200 \times 40$	1.4–2.0	2.3
UGC 1924		Nov 11, 2009	IFP 751	$180 \times 40$	1.4–2.0	2.3
UGC 3476		Nov 02, 2010	IFP 751	$220 \times 40$	1.4–1.8	2.4
UGC 3672	M 81 dwB	Nov 12, 2009	IFP 751	$160 \times 40$	1.7–3.1	3.1
UGC 5423		Feb 26, 2009	IFP 501	$180 \times 36$	2.7–2.9	3.5
UGC 5427	V II Zw 403	Mar 04, 2009	IFP 501	$180 \times 36$	2.2–2.8	3.7
UGC 6456		Nov 29, 2002	IFP 501	$300 \times 36$	1.5–2.1	2.2
UGC 7611	NGC 4460	May 19, 2010	IFP 751	$160 \times 40$	2.1–2.5	3.5
UGC 8508		May 16, 2005	IFP 501	$200 \times 36$	1.5–2.0	3.0
UGC 8638	NGC 6789	Feb 24, 2009	IFP 501	$150 \times 36$	2.8–3.5	3.9
UGC 11425		Aug 14, 2009	IFP 751	$140 \times 40$	1.5	3.0
UGC 11583		Nov 10, 2009	IFP 751	$220 \times 40$	1.2–1.6	1.9
UGC 12713		May 16, 2005	IFP 501	$200 \times 36$	3.1–3.5	3.0
UGCA 92		Nov 10, 2009	FPI 751	$180 \times 40$	1.4–1.9	2.5
UGCA 292	CVn IdwA	Feb 07, 2010	IFP 751	$120 \times 40$	2.4–3.1	3.6

the galactic core (the center of internal isophotes), then the photometric center was fixed as the center of circular rotation. For  $V_{\text{sys}}$  and  $\text{PA}_0$  we took the mean values of these parameters along the radius. In some cases, where we suspect a warp of the gas disk, variations of  $\text{PA}_{\text{kin}}$  with radius were allowed.

The inclination of the disk to the line of sight was usually fixed based on the data on the morphology of the galaxy, since the  $i_0$  estimates from the velocity fields with low rotation amplitudes are uncertain. In some cases, we still managed to estimate  $i_0$  within the assumption of the approach of pure circular rotation. In general, we tried to maximize the agreement in the orientation parameters determined according to various sources: optical imagery, HI maps, velocity fields of ionized gas (see the remarks in Section 5).

### 3.2. Disks observed edge-on

The sample includes five galaxies (UGC 231, UGC 1281, UGC 1924, UGC 3476, UGC 11583), with disk inclination almost exactly corresponding to the edge-on orientation, i.e.  $i_0 > 88^\circ$ , according the available images. The thin disk model is obviously not suitable for the description of their velocity fields. In the general case, we have to construct a 3D model of the rotating disk, taking into account the ef-

fects produced on the observed velocity field by its vertical structure, internal dust absorption, etc., as done, for example, by Kamphuis et al. (2007). However, construction of such complex models requires additional information on the morphology of galaxies at different wavelengths, which is not always available. This is why we used a simple approximation of a transparent cylinder rotating around the axis, wherein the observed line of sight velocity  $V_{\text{obs}}$  is determined, mostly, by the emission of regions located on the line passing through the center of the galaxy perpendicular to the line of sight. So that:

$$\begin{aligned} V_{\text{obs}}(x, z) &= V_{\text{rot}}(r) + V_{\text{sys}}, \\ V_{\text{rot}}(-r) &= -V_{\text{rot}}(r), \quad r = x. \end{aligned} \quad (1)$$

The  $x$  axis here is directed from the center of the galaxy along the major axis of the disk, while  $z$  is oriented orthogonally to it. This means that the shape of the rotation curve is preserved with the distance from the disk plane. We consider this approximation valid, since the observed emission disks of the studied galaxies are relatively thin (except perhaps UGC 3476). Internal dust absorption in the studied dwarf galaxies is low. At least, no contrasting dust lanes are present. Another simplification of the real situation is that ratio (1) does not account for the contribution of all emitting regions located in the line of sight. Zasov & Khoperskov (2003) show that this effect is important in the central regions of galaxies, since it makes

the observed rotation velocity gradient less steep which is especially critical for the galaxies with the central maximum on the rotation curve. But for the flat or solid-body rotation curves, typical of dwarf galaxies, the distortions of the real picture are large, especially in the outer regions.

The observed velocity fields were described by the two-dimensional model defined by expression (1), the fit parameters were the position of the rotation center,  $PA_0$  and  $V_{\text{sys}}$ . The model fitting was done by the same method as in the case of moderately inclined disks:  $\chi^2$ -minimization, masking of regions with peculiar kinematics, comparison of the positions of the kinematic and photometric centers, and so on (see the previous section). When calculating the rotation curve, the step in  $r$  was usually about  $2''$  in the center, reaching  $8\text{--}10''$  in the outer regions.

## 4. RESULTS

Figure 1 along with the original data shows the model velocity field and the result of subtracting the model from the observations. In cases where we did not manage to build a rotation model, only the initial data without subtracting the systemic velocity are listed.

Figure 2 shows the rotation curves  $V_{\text{rot}}(r)$  and diagrams of  $PA_{\text{kin}}(r)$ , calculated via the tilted-rings method. The error bars on the rotation curve correspond the mean square deviation of points in the masked field from the model (RMS). For the regions with strongly perturbed kinematics (abrupt variations of  $PA_{\text{kin}}$ , large errors in its estimates) or for those where the velocity field lacks points for the confident estimation of the position angle, we assumed  $PA_{\text{kin}} = PA_0$ . The rotation curves for the disks observed edge-on are shown in Fig. 3. Whenever possible, we compared rotation curves with the published data on the HI kinematics.

Table 2 lists the  $V_{\text{sys}}$ ,  $PA_0$ , and  $i_0$  parameters we have adopted. The error range is marked only for the parameters we measured from the ionized gas velocity fields. There the maximum rotation velocity  $V_{\text{max}}$  is also given. If the rotation curve achieves a clear plateau, then  $V_{\text{max}}$  was found as the average value of  $V_{\text{rot}}$  in this range of radii ( $r_{\text{max}}$ ). However, if the growth of rotation velocity did not stop in the outer parts of the disk, then the velocity of the most extreme point was taken for  $V_{\text{max}}$ . In this case the sign “>” shows that this is only the lower limit, and  $r_{\text{max}}$  corresponds to the distance of the considered point from the center of the galaxy.

If there was a more extended HI rotation curve present, the estimates of  $V_{\text{max}}$  were based on it, and in this case the last column of the table has a “HI” note.

## 5. NOTES ON INDIVIDUAL GALAXIES

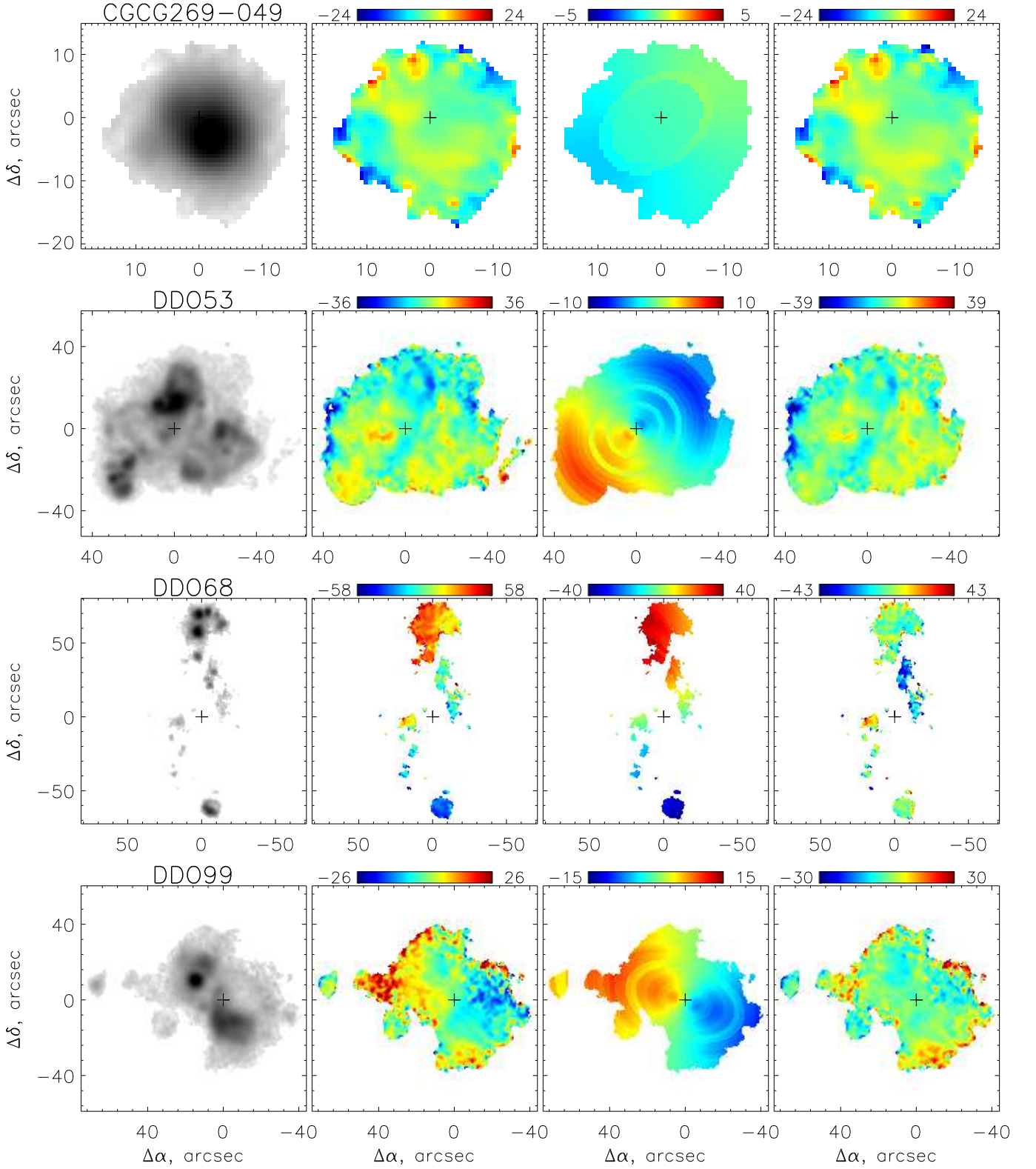
*CGCG 269-049.* Emission of ionized gas is observed only in the central part of the galaxy. The line of sight velocity gradient related with circular rotation is hardly noticeable. The velocity field is dominated by peculiar motions, most

likely related to the nuclear HII region (outflows or an expanding shell). Meanwhile, according to Begum et al. (2006), the HI kinematics at large distances from the center follows regular rotation, although the disturbance from the star-forming region is also noticeable in the HI velocity field. We took the same value of  $i_0$  that was measured in Begum et al. (2006) from the HI maps, it is well consistent with the optical image of the galaxy. The  $PA_0$  estimate is taken from the HyperLeda.<sup>2</sup> The model created with these parameters indicates that the ionized gas rotation velocity is formally very low, less than  $2 \text{ km s}^{-1}$  for  $r < 12''$ . We have constructed the HI rotation curve, shown for comparison in Fig. 2, via the tilted-rings method from the velocity field, kindly provided by the authors of Begum et al. (2006). Here for  $r < 30''$  a field with the resolution of beam =  $28'' \times 24''$  was used, while for the outer regions they have used the data with a lower resolution (beam =  $42'' \times 37''$ ).

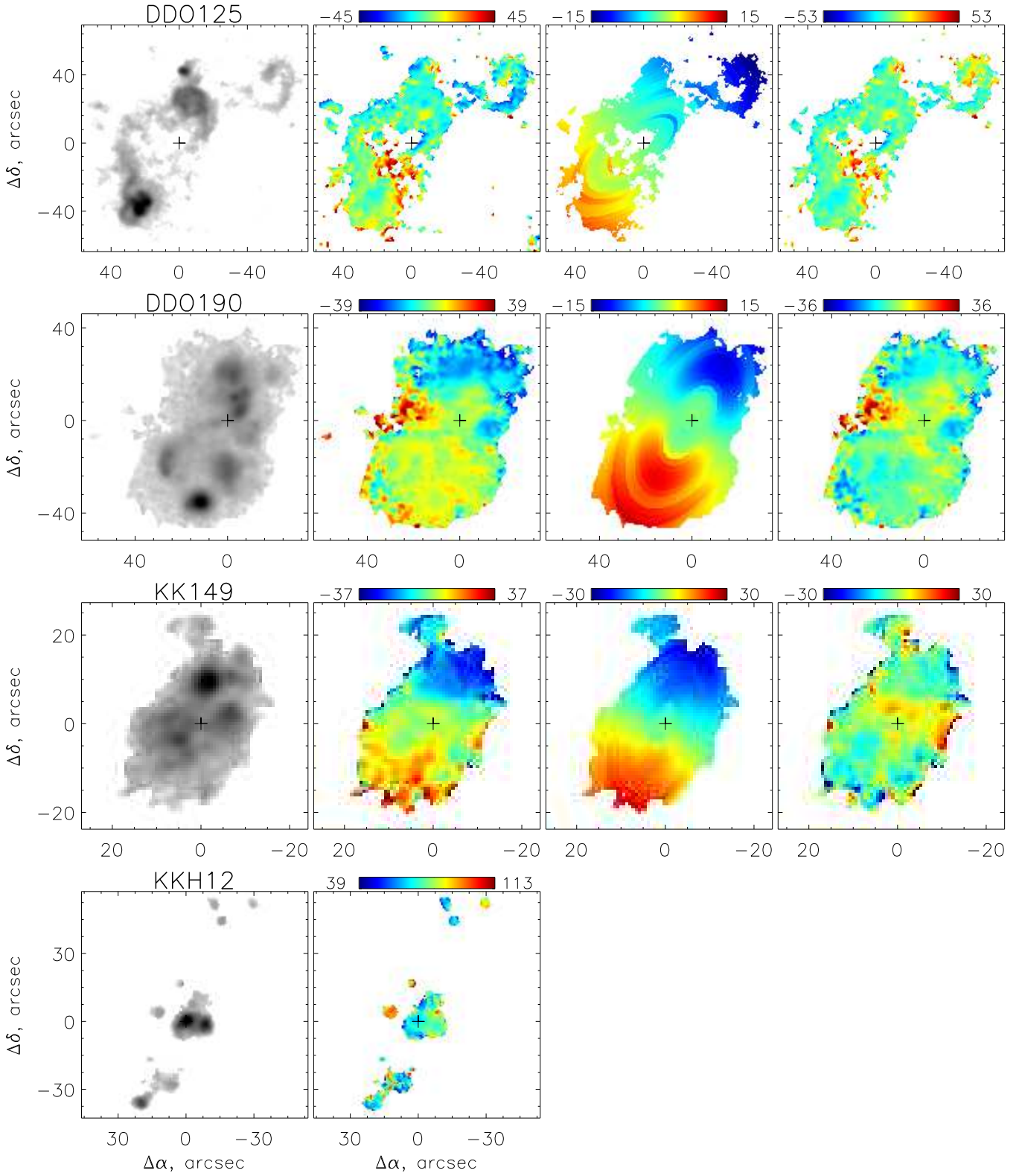
*DDO 53.* We have earlier discovered several expanding shells in this galaxy (Moiseev & Lozinskaya, 2012). At the first glance, the velocity field looks chaotic. But after masking peculiar regions it reveals a regular line of sight velocity gradient, consistent with the pattern observed with a lower spatial resolution in the HI (Begum et al., 2006; Oh et al., 2011). The orientation parameters were taken based on the measurements of Oh et al. (2011) from the neutral hydrogen velocity field. Note that the measurements from the  $H\alpha$  velocity field give a close value of the position angle:  $PA_{\text{kin}} = 127 \pm 8^\circ$ . The rotation curves in HI and HII agree within errors, except for the outer regions of the disk in  $H\alpha$ , where the HI rotation curve reaches plateau.

*DDO 68.*  $H\alpha$  emission is observed only in individual HII regions, but the line of sight velocity gradient is clearly visible in the north–south direction. The disk orientation parameters cannot be measured based on our data. We hence took the photometric estimates of Hunter & Elmegreen (2006) for  $PA_0$  and  $i_0$ , which are in a satisfactory agreement with the HI maps given in Ekta et al. (2008). The map of residual velocities (Fig. 2) reveals notable peculiar velocities only in the regions north of the center, at  $r \approx 10\text{--}40''$ . This might be caused by the imperfections of our model, since due to the lack of significant points in this region, solid-body rotation, followed by reaching the plateau, was assumed. Unfortunately, the authors of Ekta et al. (2008) give an HI rotation velocity estimate only at two points on the opposite sides of the nucleus. A comparison with the measurements of Hoffman et al. (1996), based on the maps obtained at the Arecibo radio telescope, shows that the HII rotation velocity at the same  $r$  is systematically lower than the neutral hydrogen data (Hoffman et al., 1996, we recomputed their data to  $i_0 = 65^\circ$ ). The difference is possibly caused by the lack of HII regions located along the major axis of the galaxy. Hence, the uncertainty in the  $PA_0$  estimate leads to a decrease in  $V_{\text{rot}}$ . Besides, ac-

<sup>2</sup> <http://leda.univ-lyon1.fr>

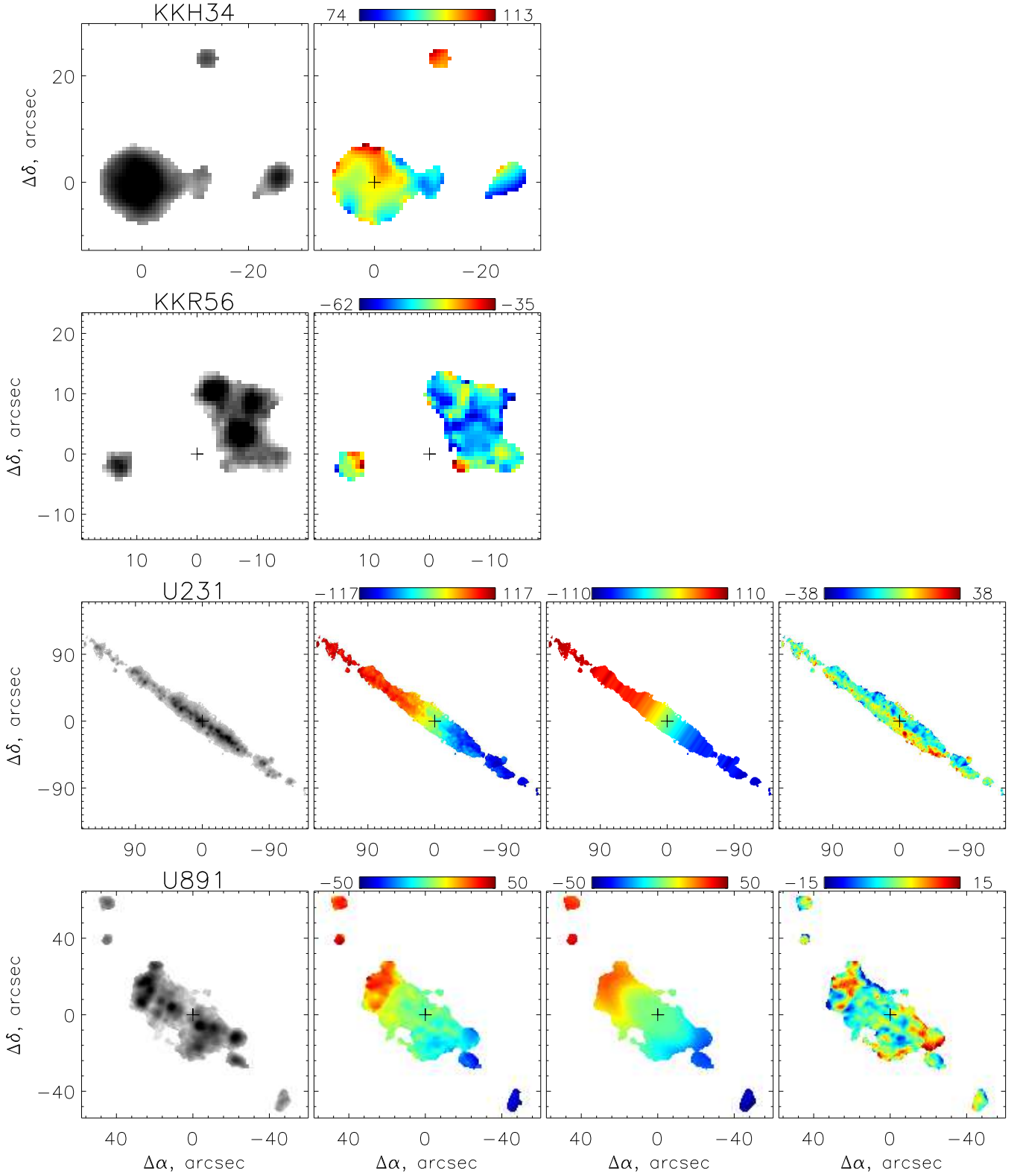


**Fig. 1.** The results of observations and analysis within the assumption of circular rotation. From left to right: the H $\alpha$  line image, the line of sight velocity field (systemic velocity  $V_{\text{sys}}$ , listed in Table 2, is subtracted), model velocity field, residual velocity field (observations minus model). The cross marks the position of the kinematic center. The scale is in  $\text{km s}^{-1}$ .

**Fig. 1.** (Contd.)

cording to Ekta et al. (2008), the morphological and kinematic features of HI suggest that the galaxy has experi-

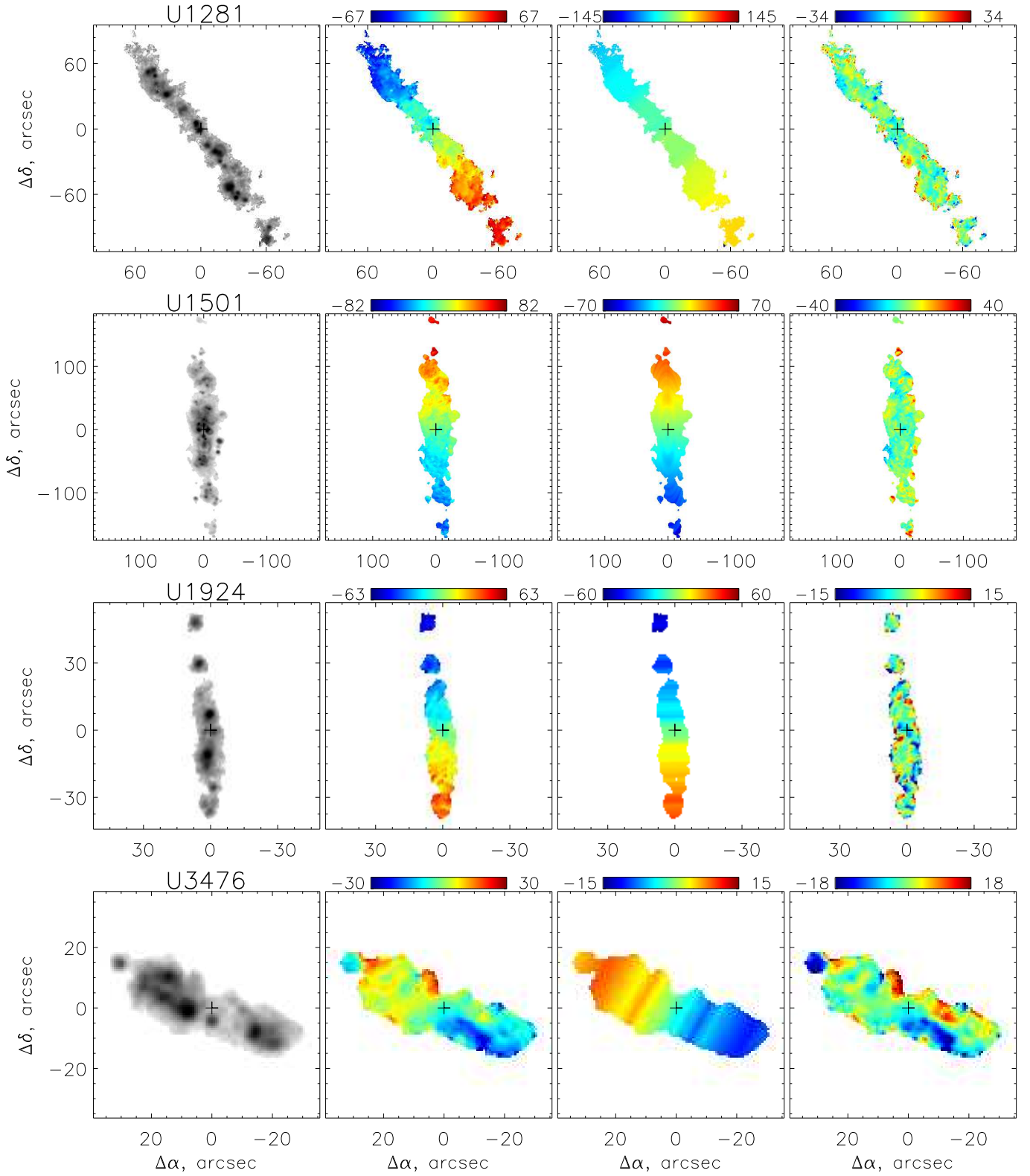
enced a recent interaction leading to the perturbation of its gaseous disk.

**Fig. 1.** (Contd.)

*DDO 99.* The disk orientation parameters are taken from the photometric estimates of Fingerhut et al. (2010). The velocity field is well filled, the velocities of the ma-

jority of regions of the disk correspond to the circular rotation model. The values of  $PA_{\text{kin}}$  we have measured are within the errors consistent with the adopted  $PA_0$  (Fig. 2).

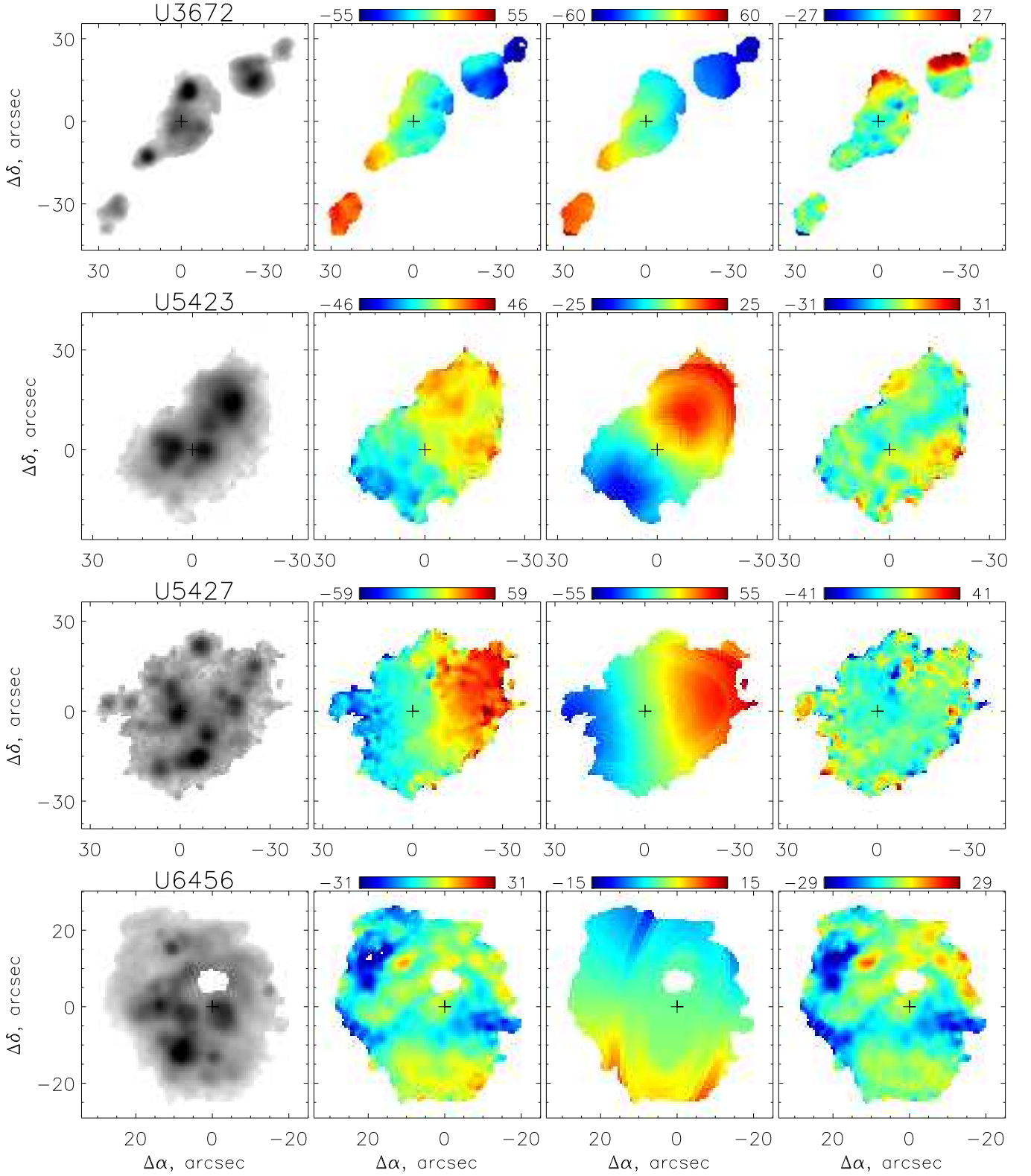


**Fig. 1.** (Contd.)

Hence, even more surprising is the comparison with the published HI maps. On the one hand, the HI surface density distribution of Begum et al. (2008); Ott et al. (2012)

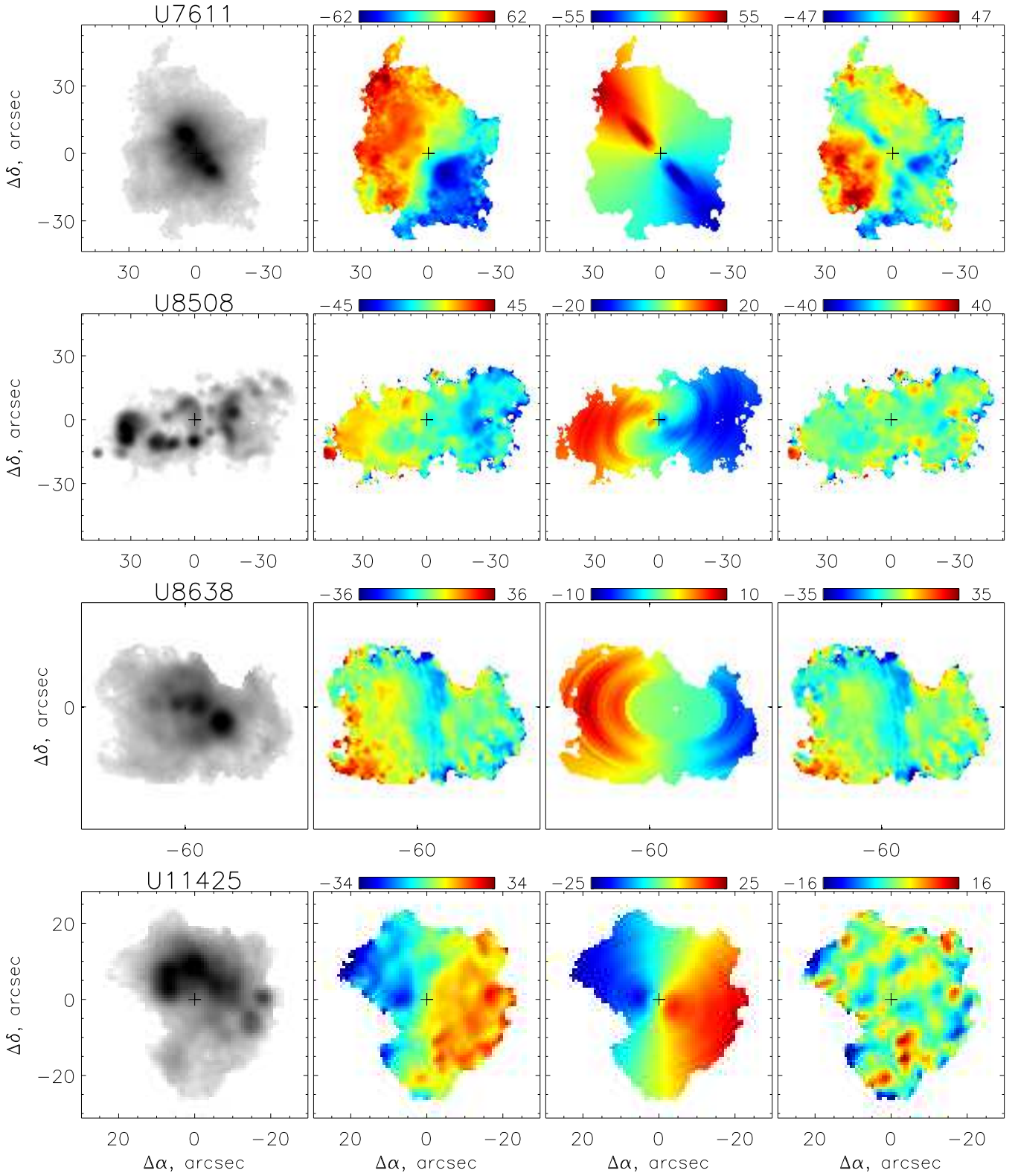
agrees well with the optical morphology, i.e., it is elongated along the  $PA = 60\text{--}70^\circ$ . On the other hand, in the HI velocity field (see Fig. 17 in Ott et al., 2012),  $PA_{\text{kin}}$



**Fig. 1.** (Contd.)

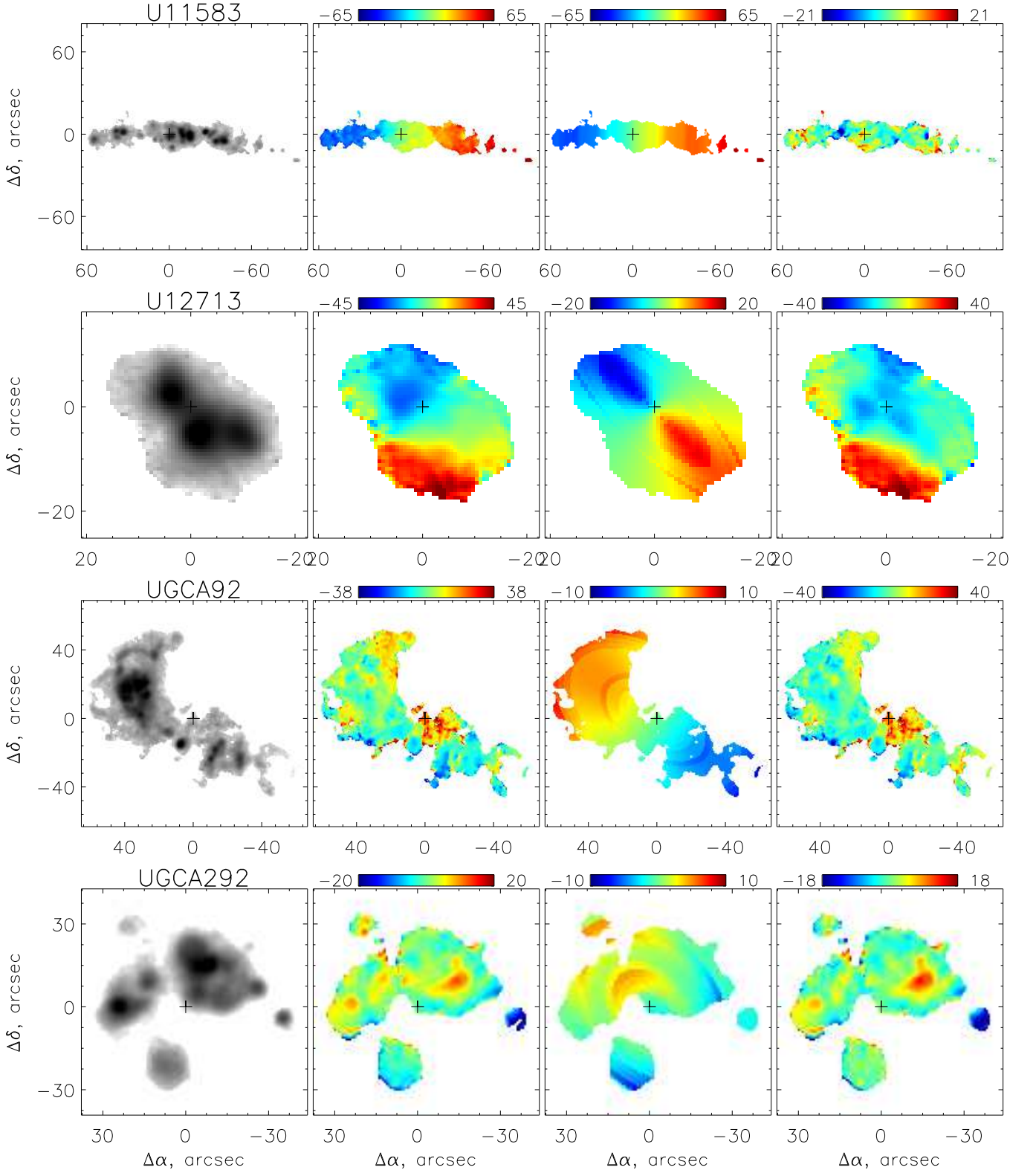
is turned almost perpendicularly to the major axis in the density distribution so that  $PA_{\text{kin}} = 130\text{--}150^\circ$ . And the rotation velocity is at least  $25\text{--}30 \text{ km s}^{-1}$  which is signifi-

cantly higher than our estimates from H II. This discrepancy between the morphology and kinematics can indicate that the disk of neutral hydrogen is non-stationary, it was

**Fig. 1.** (Contd.)

formed relatively recently as a result of interaction or external accretion and rotates in a plane, strongly inclined to the main galaxy. At that, the orbits of gas clouds in the

inner regions have already precessed in the plane of the stellar disk which is exactly what we see in the ionized gas.

**Fig. 1.** (Contd.)

*DDO 125.* The  $H\alpha$  image is flocky, numerous expanding shells are identified in it (Moiseev & Lozinskaya, 2012). At the same time, radial velocities are in a

reasonable agreement with the circular rotation model. The galaxy has been mapped in HI many times (see Swaters et al., 2009; Begum et al., 2008; Ott et al., 2012,

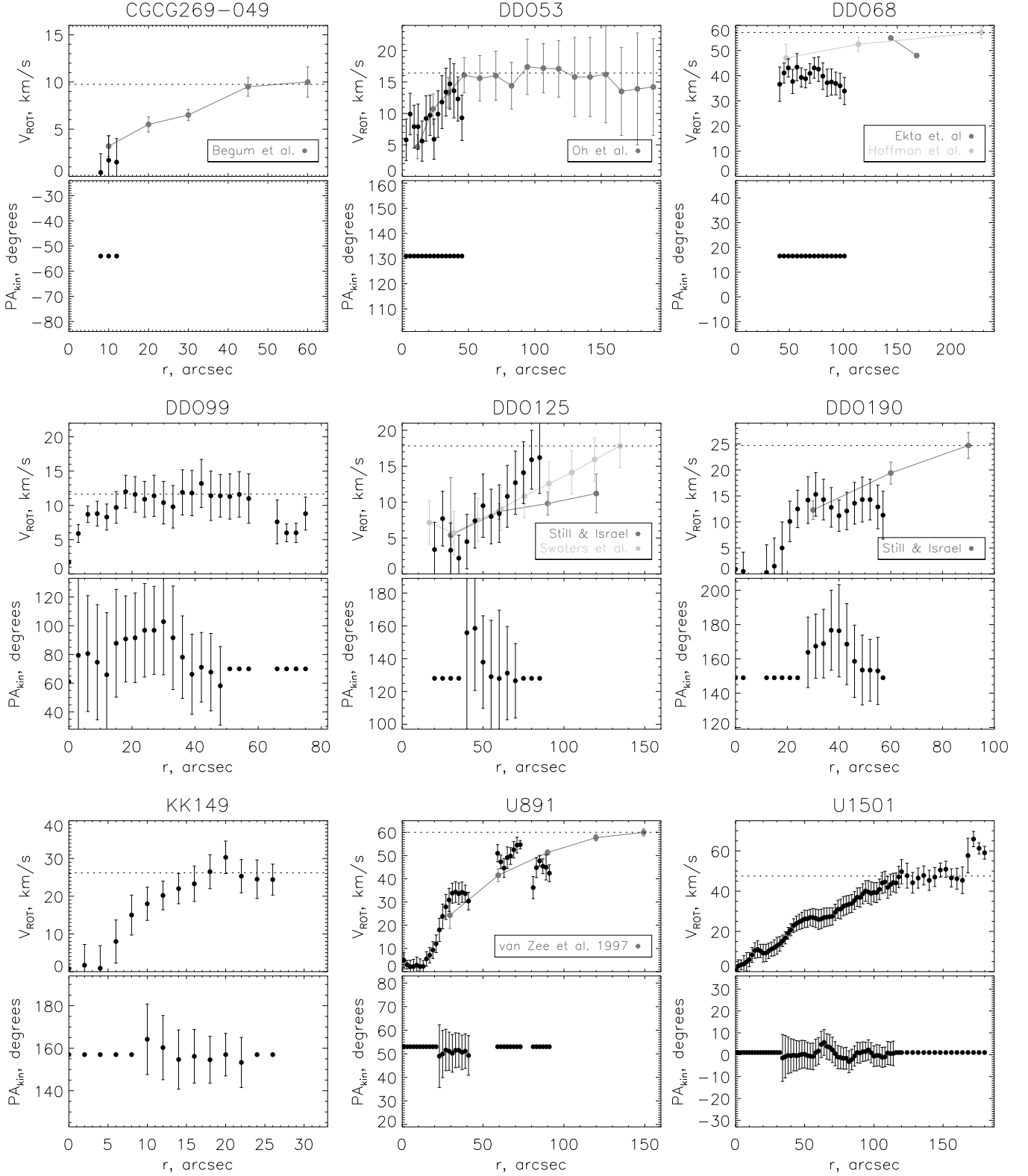


**Fig. 2.** Rotation curves and radial variations of  $PA_{\text{kin}}$  for the galaxies with moderately inclined disks. Black circles represent our measurements from the velocity fields in  $H\alpha$ , gray circles mark the literature data. The dashed line marks the adopted  $V_{\text{max}}$  value.

ibid the references to earlier work). We have taken the same  $PA_0$  and  $i_0$  that were measured in Swaters et al. (2009) based on the velocity field of neutral hydrogen. The

HI and HII rotation curves agree within errors. Relative growth of rotation velocity in  $H\alpha$  by  $r > 70''$  is likely an

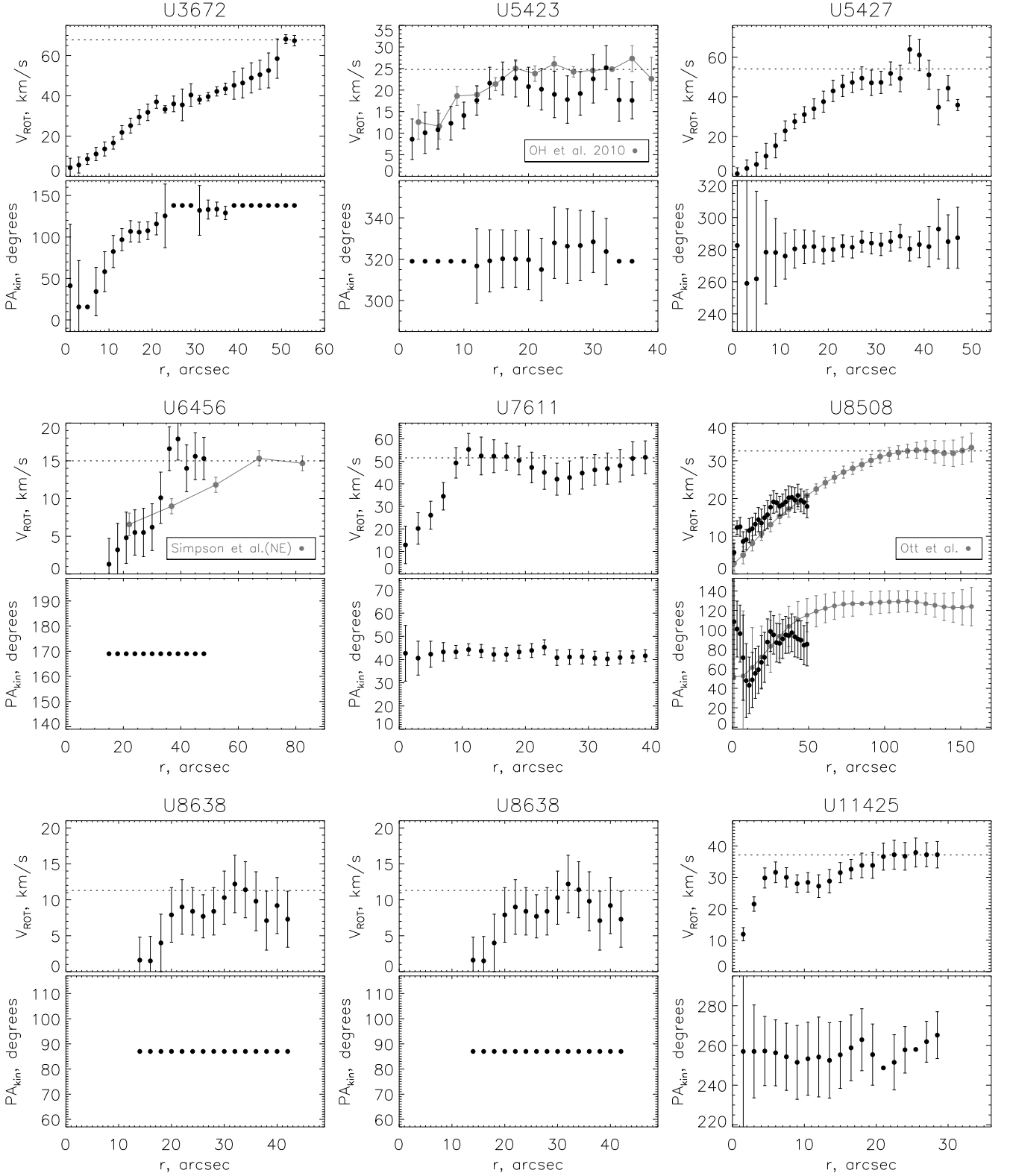


**Fig. 2.** (Contd.)

artifact related with non-circular motions in the north-western star-forming region.

*DDO 190.* At  $r \leq 20''$  rotation of ionized gas is almost not observed, since peculiar motions dominate there. At large distances from the center, the velocity field follows

the circular rotation model with the orientation parameters fixed in the HI observations of Stil & Israel (2002). The residual velocity field reveals an area along the minor axis of the galaxy as well as separate ionized shells.

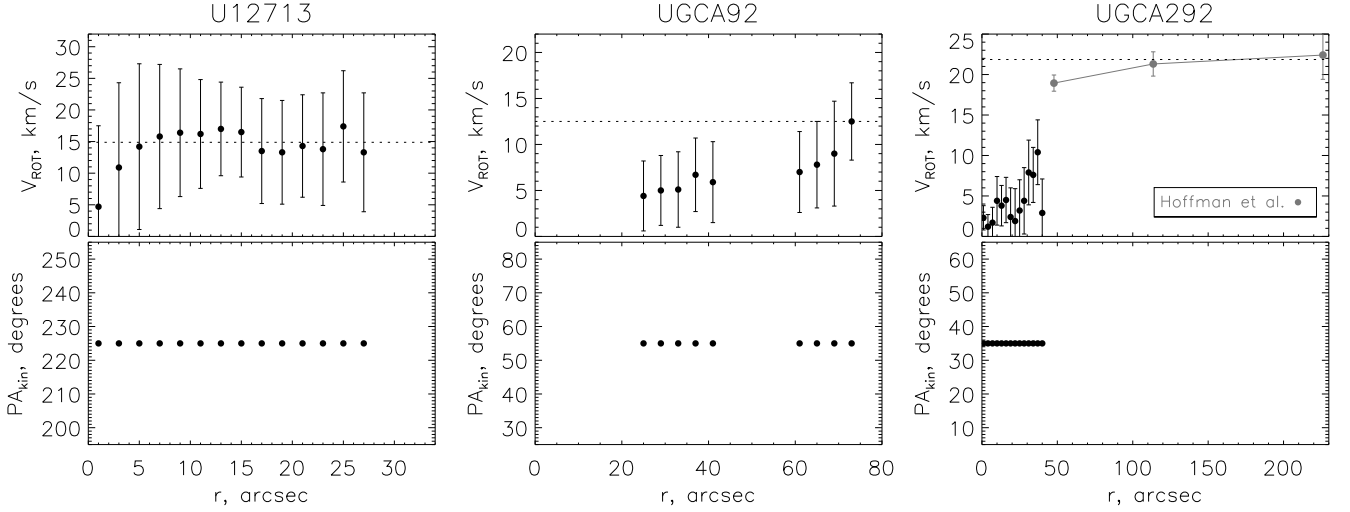


Fig. 2. (Contd.)

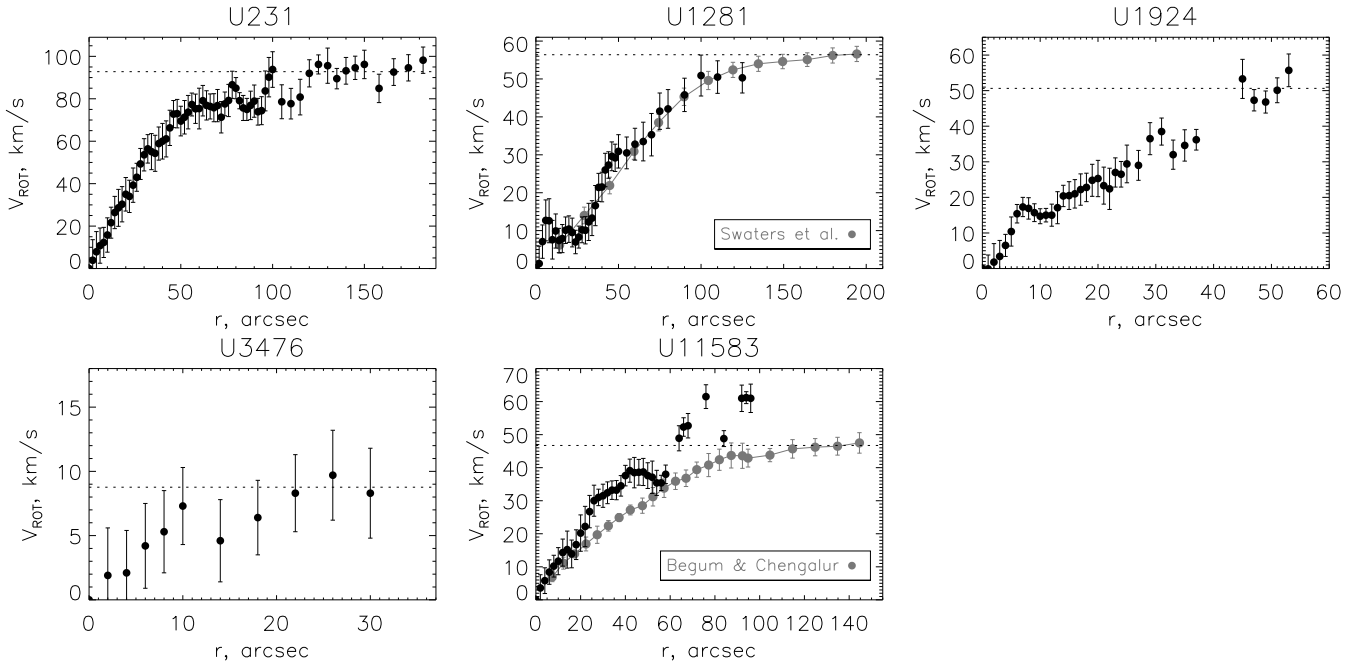


Fig. 3. Rotation curves of the edge-on galaxies. The markings are the same as in Fig. 2.

The H II rotation curve reaches plateau at  $r > 30''$ , while a more extended curve in HI shows further growth.

*KK149*. Ionized gas rotation is almost lacking in the innermost region ( $r \leq 5''$ ). At larger distances, the velocity field follows circular rotation. The residual velocity field has noticeable disturbances associated with the shells around the H II regions. We took the HyperLeda data for  $i_0$  because from the kinematics the inclination is estimated with a great uncertainty. At the same time, the positional angle measured from the velocity field is in a good agreement with the available photometric estimates.

*KKH12*, *KKH34*, and *KKR56*. Only separate compact H II regions are observed here. The rotation model failed to be created.

*UGC231*. After subtracting the “rotating cylinder” model from the observed velocity field, the residual velocities in the northwestern part of the disk are systematically lower than those in the south-east. This most likely implies small deviations ( $0.5\text{--}1^\circ$ ) of the inclination from  $i = 90^\circ$ . The rotation curve we constructed is in a good agreement with the measurements based on ionized gas from de Blok & Bosma (2002). At that, our measurements extend farther on, to  $r \approx 180''$ . According to the observations of Rhee & van Albada (1996), the HI disk is observed up to  $r \approx 300''$ , where the maximum rotation velocity amounts to  $98 \pm 3 \text{ km s}^{-1}$  which is close to our estimate.

*UGC891*. van Zee et al. (1997) have obtained from the HI observations  $i = 60 \pm 5^\circ$  and  $\text{PA} = 48 \pm 2^\circ$ , what is

normal

**Table 2.** Galaxy parameters

Name	$V_{\text{sys}}, \text{ km s}^{-1}$	$\text{PA}_0, \text{ deg}$	$i_0, \text{ deg}$	$V_{\text{max}}, \text{ km s}^{-1}$	$r_{\text{max}}, \text{ arcsec}$	Note
CGCG 269-049	$139 \pm 1$	306	43	$9.8 \pm 0.9$	45–60	HI
DDO 53	$27 \pm 2$	131	27	$16.4 \pm 2.6$	106–153	HI
DDO 68	$511 \pm 1$	17	65	$> 57.2 \pm 2.2$	228	HI
DDO 99	$249 \pm 1$	70	52	$11.7 \pm 1.4$	42–57	
DDO 125	$200 \pm 1$	128	63	$> 17.8 \pm 3.0$	134	HI
DDO 190	$153 \pm 2$	149	60	$> 24.7 \pm 2.5$	90	HI
KK 149	$410 \pm 2$	$157 \pm 5$	58	$26.2 \pm 2.0$	18–26	
KKH 12	–	–	–	–	–	
KKH 34	–	–	–	–	–	
KKR 56	–	–	–	–	–	
UGC 231	$835 \pm 2$	$56 \pm 3$	90	$92.8 \pm 2.2$	120–158	
UGC 891	$637 \pm 1$	$53 \pm 2$	$65 \pm 3$	$> 60.0 \pm 1.6$	149	HI
UGC 1281	$140 \pm 1$	$220 \pm 1$	90	$56.4 \pm 1.4$	179–194	HI
UGC 1501	$183 \pm 2$	$1 \pm 2$	75	$47.5 \pm 1.5$	120–160	
UGC 1924	$586 \pm 1$	$181 \pm 1$	90	$50.6 \pm 1.8$	45–53	
UGC 3476	$439 \pm 3$	$60 \pm 3$	$90 \pm$	$8.8 \pm 1.9$	22–30	
UGC 3672	$984 \pm 3$	138	56	$67.8 \pm 1.7$	51–53	
UGC 5423	$354 \pm 1$	$319 \pm 3$	$56 \pm 5$	$24.8 \pm 0.9$	20–39	HI
UGC 5427	$484 \pm 3$	$281 \pm 4$	$55 \pm 5$	$54.1 \pm 2.8$	31–41	
UGC 6456	$-116 \pm 2$	169	66	$15.0 \pm 0.7$	67–82	HI
UGC 7611	$487 \pm 1$	$42 \pm 2$	77	$51.5 \pm 5.2$	37–39	
UGC 8508	$60 \pm 2$	$126 \pm 3$	$51 \pm 3$	$32.6 \pm 1.2$	121–157	HI
UGC 8638	$275 \pm 1$	87	49	$11.3 \pm 2.2$	30–34	
UGC 11583	$113 \pm 2$	$268 \pm 1$	90	$46.7 \pm 1.6$	124–144	HI
UGC 11425	$-167 \pm 2$	$255 \pm 5$	35	$37.1 \pm 1.8$	21–28	
UGC 12713	$285 \pm 2$	225	72	$14.9 \pm 2.9$	13–27	
UGCA 92	$-108 \pm 2$	$55 \pm 5$	56	$> 12.5 \pm 4.2$	73	
UGCA 292	$297 \pm 1$	35	45	$21.9 \pm 1.7$	113–226	HI

close to the disk orientation parameters we have measured. As in the cases of DDO 190 and KK 149, rotation of ionized gas in the central region is almost imperceptible here. At  $r > 20''$ , the H II kinematics follows the model of regular rotation. The velocities of external isolated H II regions are consistent with a more extended rotation curve in HI (van Zee et al., 1997).

*UGC 1281.* A good agreement with the approach of the rotating cylinder. The H II rotation curve perfectly fits with the measurements in HI (Swaters et al., 2009).

*UGC 1501.* From the analysis of the velocity field, we have obtained  $i = 65 \pm 5^\circ$ ,  $\text{PA} = 1 \pm 2^\circ$ . But this  $i$  value looks clearly underestimated, since the outer galaxy isophotes correspond to a greater inclination. Therefore, we have adopted  $i_0 = 75^\circ$  according to the photometry in van Zee (2000). The ionized gas velocity field was also presented by Kandalyan et al. (2003), but our measurements are deeper. The rotation velocity step at  $r > 170''$  was not included in the  $V_{\text{max}}$  estimate, since it corresponds only to one most external H II region north of the nucleus.

*UGC 1924.* A good agreement with the approach of the rotating cylinder. The  $V_{\text{max}}$  estimate is made by the outer H II region, since unlike in UGC 1501, these points correspond to the linear extrapolation of the rotation curve at smaller  $r$ .

*UGC 3476.* It is possible that the inclination of the galaxy differs by several degrees from the accepted  $i_0 = 90^\circ$ . The residual velocity field at the boundaries of the bright H II regions reveals noticeable local deviations of up to  $20\text{--}30 \text{ km s}^{-1}$ . The measured maximum rotation velocity is 2–3 times lower than that expected from the Tully-Fisher relation for a galaxy with  $M_B = -14$ . The rotation velocity most likely reaches its maximum outside the H $\alpha$ -emitting disk.

*UGC 3672.* The disk parameters are taken according to the photometric estimates of van Zee (2000) because the velocity field is strongly perturbed. Rotation with  $\text{PA}_{\text{kin}}$  close to  $\text{PA}_0$  is observed only for  $r > 23''$ . The direction of the velocity gradient in the central region of the galaxy varies the way that  $\text{PA}_{\text{kin}}$  sharply decreases (Fig. 2). Consider the possible explanations of this kinematics:

1. Significant non-circular motions of gas. This way,  $\text{PA}_{\text{kin}}$  may dramatically change in the case of radial motions under the effect of the bar non-axisymmetric potential (see discussion and references in Moiseev et al., 2004)). But even in this case, a change in  $\text{PA}_{\text{kin}}$  by almost  $90^\circ$  is extraordinary. In addition, the bar is not visible in the optical images. The assumption of the outflow of gas under the effect of vigorous star formation leaves doubts since there are no bright H II regions in the core. Furthermore, in



this case we should expect a significant increase of gas velocity dispersion or even the splitting of the  $H\alpha$  line profile which is not observed.

2. Rotation in the plane different from the stellar disk of the galaxy. Our estimate shows that the circumnuclear velocity field can be described in the assumption that  $PA = 84 \pm 6^\circ$ . This means that there is an internal inclined or even polar disk. Such structures are observed in a number of nearby galaxies, including dwarf (see Moiseev, 2012, for review)). However, the brightness distribution in the line of  $H\alpha$  for the central region of UGC 3672 corresponds to  $PA = 120\text{--}150^\circ$  which is closer to the orientation of the major axis of the stellar disk than to  $PA$  of the presumed polar structure.
3. The observed structure is not stationary, it is a result of the tidal effect or of the capture of the destroyed companion's matter. It may possibly be a polar structure in the process of formation.

*UGC 5423.* The orientation parameters we have obtained coincide within the errors with the measurements of Daigle et al. (2006), based on the ionized gas velocity field. The rotation curve we have constructed extends further than in Daigle et al. (2006). Oh et al. (2011) obtained the mean value of  $i_0 = 44^\circ$  from the HI velocity field, but they noted that the inclination of the disk expected from the Tully-Fisher baryon relationship has to be much larger and amount to  $59^\circ$ . Therefore, we consider our  $i_0 = 56^\circ$  estimate to be more correct and better corresponding to the isophote ellipticity in the image of the galaxy. The HI rotation curve, demonstrated in Fig. 2, was recalculated from Oh et al. (2011) to the taken  $i_0$ . Only the points up to  $r = 1$  kpc ( $39''$ ) are shown there, as at large distances from the center, according to the authors, their estimates are uncertain.

*UGC 5427.* A good agreement with the approach of circular rotation, except for certain regions of low surface brightness. A decrease of rotation velocity at  $r > 40''$  is most likely an artifact, since there exist measurements only for the eastern half of the disk.

*UGC 6456.* A well-known blue compact galaxy with numerous ionized shells around the star forming regions (Simpson et al., 2011; Moiseev & Lozinskaya, 2012, *ibid* the references to earlier work).  $PA_0$ ,  $i_0$  were taken according to the photometric estimate of Simpson et al. (2011). The same article gives the HI velocity field. However, the orientation parameters based on the kinematics of neutral hydrogen are determined with great uncertainty, since the velocity field is perturbed and asymmetrical which may be the result of tidal interaction. However, the maximum rotation velocity from HI and HII prove to be close (see Fig. 2, where the HI rotation curve for the north-west half of the galactic disk is shown for comparison). The deviations of line of sight velocities in  $H\alpha$  from the circular rotation model are related both with the individual expanding shells and with the overall asymmetry of the gaseous disk, noted in Simpson et al. (2011).

*UGC 7611.* Kaisin & Karachentsev (2008) have discovered that the emission of ionized gas is observed not only around the regions of star formation but also far beyond the strongly inclined disk of the galaxy. Further spectroscopic observations (Moiseev et al., 2010a) have shown that the extended emission nebula is composed of galactic wind, i.e., gas ejected from the plane of the disk as a result of a cumulative effect of stellar winds and supernova explosions. At that, in the disk itself, according our velocity, the kinematics of ionized gas is in a good agreement with the circular rotation model. The  $i_0$  value is taken according to the photometric estimate from Moiseev et al. (2010a),  $PA_0$  is calculated from the velocity field. In the regions where the galactic wind is present, line of sight velocities significantly (up to  $50 \text{ km s}^{-1}$ ) differ from what the extrapolation of the circular rotation model. Obviously, models that are kinematically more complex need to be applied here, taking into account the geometry and speed of the outflow.

*UGC 8508.* If the pronounced velocity gradient observed in the HII velocity field results from circular rotation, it corresponds to  $PA_{\text{kin}} = 80\text{--}100^\circ$ . At that, the image of the galaxy itself in the line of  $H\alpha$  is extended along this direction. However, such a  $PA$  drastically differs from the outer isophote major axis orientation in the optical image of the galaxy ( $PA = 123^\circ$ , HyperLeda). The density distribution in HI at large distances from the center is also extended along  $PA = 115\text{--}120^\circ$  (see the maps in Begum et al., 2008; Ott et al., 2012). Thus, the situation here is similar to the above-described cases of the disagreement of kinematic parameters in the inner and outer regions of DDO 99 and UGC 3672. Compared with these galaxies, UGC 8508 reveals the most regular motions of ionized gas. We have earlier identified two giant ionized shells as well as a nebula around a candidate LBV star (Moiseev & Lozinskaya, 2012). But their contribution to the perturbation of the velocity field is small, and while constructing the model, these regions were excluded from consideration. We used the tilted-rings method to make an analysis of the HI velocity field obtained at the VLA with the resolution of  $14 \times 12''$ . The orientation parameters for the outer regions of the disk ( $r > 80''$ ) are given in Table 2 and agree well with the above photometric estimates. However, at  $r < 50''$  there is a sharp reversal of  $PA_{\text{kin}}$ , while its measurements in HI and HII coincide. We have therefore adopted for UGC 8508 a model of a gas layer warped in the inner part, ensuing from the plane of the stellar disk of the galaxy. Similar strong internal warps are observed, for example, in the gaseous disks of the lenticular galaxy NGC 2685 (Jzsa et al., 2009) and the dwarf galaxy Mrk 370 (Moiseev, 2011). If we accept for the disk of ionized gas of UGC 8508  $PA \approx 90^\circ$ ,  $i \approx 50^\circ$ , then the calculation of the angle between the planes of the stellar disk and the HII disk (see the formula in Moiseev, 2008) would yield two values:  $28^\circ$  and  $86^\circ$ . The latter value corresponds almost exactly to the orthogonal mutual orientation, i.e., UGC 8508 possibly includes an internal polar disk.

*UGC 8638.* The velocity field is well filled by the H $\alpha$  emission, but it is quite difficult to separate the regular rotation and peculiar motions. The orientation parameters of the disk are taken from the HyperLeda.

*UGC 11425.* The velocity field is dominated by regular circular rotation. The inclination is adopted in accordance with the photometry from Hunter & Elmegreen (2006),  $PA_0$  was refined from the velocity field.

*UGC 11583.* The velocity field is described well by the rotating cylinder model, but the H II rotation curve does not always coincide with a more extended HI rotation curve from Begum & Chengalur (2004). Firstly, the plateau in H II is reached at the smaller distances  $r = 40''$ , which is possibly related with a better spatial resolution of our data. A faster rotation velocity in H $\alpha$  at  $r = 60\text{--}100''$  corresponds to the chain of H II regions at the western edge of the disk. It is difficult to understand why their radial velocities are by  $15\text{--}20\text{ km s}^{-1}$  greater than the maximum rotation velocity. They possibly belong to a tidal structure.

*UGC 12713.* The disk orientation parameters are taken according to the analysis of HI maps in Noordermeer & van der Hulst (2007). The ionized gas velocity field reveals a notable reversal of isovels. The velocities on the southern edge of the disk vary from the circular model by more than  $30\text{ km s}^{-1}$ . The tidal perturbation is the most likely explanation for such peculiar motions.

*UGCA 92.* The H $\alpha$  emission is mainly observed in numerous expanding ionized shells (Moiseev & Lozinskaya, 2012). The contribution of regular rotation in the velocity field is negligible, but we able to calculate the rotation curve. The  $i_0$  is taken in accordance with the observations in HI (Begum et al., 2008). The HI density distribution outside the optical disk is complex, external HI isodenses are turned almost perpendicularly to the optical image. For  $PA_0$  our estimate is given from the isophotes of the POSS2 image.

*UGCA 292* The galaxy with an extended disk of neutral hydrogen, the corresponding maps are shown in Lo et al. (1993); Young et al. (2003). Unfortunately, the H $\alpha$  line reveals only a few H II regions near the center of the galaxy. Rotation velocity of ionized gas does not exceed  $10\text{ km s}^{-1}$  which is two times smaller than the maximum velocity of rotation in HI, shown in Fig. 2 according to Hoffman et al. (1996) (the data are recomputed to the taken  $i_0$ ). The  $i_0$  estimate is adopted from Young et al. (2003), and  $PA_0$ —from Lo et al. (1993).

## 6. CONCLUSION

We have constructed and analyzed the ionized gas velocity fields in 28 nearby dwarf galaxies. These results (rotation curves, maximum rotation velocity estimates) can be useful for studying the mass distribution in these objects. Specifically, they are already used in our paper (Moiseev, Tikhonov & Klypin, 2014). Note some

points concerning the internal kinematics of galaxies considered:

1. The ionized gas velocity perturbation amplitude in dwarf galaxies under the effect of the star formation may even exceed the rotation velocity. However, in the majority of cases (in 25 galaxies) we can successfully identify the kinematic component associated with regular circular rotation. The H II rotation curves we have constructed are generally in a good agreement with data measured from neutral hydrogen, taking into account the spatial resolution difference.
2. In several cases, rotation pattern of ionized gas is very different from the one that should be expected from the orientation of external optical isophotes or the large-scale HI velocity field. In DDO 99, for instance, the inner part of the gaseous disk, observed in the H $\alpha$  emission line, lies in the stellar disk plane, while the external gas, observed in the 21 cm line is out of this plane. These structures are most likely the result of interaction with a companion or external accretion of gas. The traces of tidal perturbations are visible in the velocity fields of UGC 6456, UGC 11583, UGC 12713, and UGC 3672. In the latter case, it seems that the inner part of the disk of ionized gas rotates at a large angle to the stellar disk. The variation of orbit orientation of gas clouds can be most thoroughly traced in the UGC 8508. Here the external HI disk coincides with the plane of the stellar disk, but in the inner region we observe a warp of the gas layer, traced both in the HI and H II. It is possible that the entire ionized gas in the UGC 8508 rotates in the plane orthogonal to the stellar disk of the galaxy.

*Acknowledgements.* This work was carried out with the financial support of the non-profit Dynasty Foundation, the program of the Ministry of Education and Science of Russian Federation (project 8523), the RFBR grant no. 13-02-00416, and the Basic Research Program of the RAS Division of Physical Sciences OFN-17 “Active Processes in the Galactic and Extragalactic Objects. We used the NASA/IPAC (NED) database of extragalactic data, managed by the Jet Propulsion Laboratory of the California Institute of Technology under the contract with the NASA (USA), and the HyperLeda database. The paper is based on the observational data of the 6-m telescope of the Special Astrophysical Observatory of RAS operating with the financial support from the RF Ministry of Education and Science (state contracts no. 16.518.11.7073 and 14.518.11.7070). The author thanks Jayaram Chengalur and Ayesha Begum, who have kindly presented the original data published in their papers, and Anatoly Klypin and Simon Pustilnik for useful discussions.

## References

- Afanasiev V.L., & Moiseev A.V., 2005, *Astronomy Letters*, 31, 194  
 Begum A., & Chengalur J.N., 2004, *A&A*, 424, 509  
 Begum A., Chengalur J.N., Karachentsev I.D., et al., 2006, *MNRAS*, 365, 1220

- Begum A., Chengalur J.N., Karachentsev I.D., et al., 2008, MNRAS, 386, 1667
- Daigle O., Carignan C., Amram P., et al., 2006, MNRAS, 367, 469
- de Blok W.J.G., & Bosma A., 2002, A&A, 385, 816
- Doroshkevich A.G., Lukash V.N., & Mikheeva E.V., 2012, Physics Uspekhi, 55, 3
- Ekta B., Chengalur J.N., & Pustilnik S.A., 2008, MNRAS, 391, 881
- Epinat B., Amram P., & Marcelin M., 2008, MNRAS, 390, 466
- Fingerhut R.L., McCall M.L., Argote M., et al., 2010, ApJ, 716, 792
- Hoffman G.L., Salpeter E.E., Farhat B., et al., 1996, ApJS, 105, 269
- Hunter D.A., & Elmegreen B.G., 2006, ApJS, 162, 49
- Hunter D.A., Ficut-Vicas D., Ashley T., et al., 2012, AJ, 144, 134
- Jzsa G.I.G., Oosterloo T.A., Morganti R., et al., 2009, A&A, 494, 489
- Kaisin S.S., & Karachentsev I.D., 2008, A&A, 479, 603
- Kamphuis P., Peletier R.F., Dettmar R.-J., et al., 2007, A&A, 468, 951
- Kandalyan R.A., Khassawneh A.M., & Kalloghlian A.T., 2003, Astrophysics, 46, 74
- Lozinskaya T.A., Moiseev A.V., Avdeev V.Y., Egorov O.V., 2006, Astronomy Letters, 32, 361
- Lo K.Y., Sargent W.L.W., & Young K., 1993, AJ, 106, 507
- Moiseev A.V., 2002, BSAO, 54, 74
- Moiseev A.V., 2008, Astrophysical Bulletin, 63, 201
- Moiseev A., 2011, in *EAS Publications Series*, Vol. 48, 115
- Moiseev A.V., 2012, Astrophysical Bulletin, 67, 147
- Moiseev A.V., & Egorov O.V., 2008, Astrophysical Bulletin, 63, 181
- Moiseev A.V., & Lozinskaya T.A., 2012, MNRAS, 423, 1831
- Moiseev A.V., Valdés J.R., & Chavushyan V.H., 2004, A&A, 421, 433
- Moiseev A., Karachentsev I., & Kaisin S., 2010, MNRAS, 403, 1849
- Moiseev A.V., Pustilnik S.A., & Kniazev A.Y., 2010, MNRAS, 405, 2453
- Moiseev A.V., Tikhonov A.V., & Klypin A., 2014, MNRAS, submitted
- Noordermeer E., & van der Hulst J. M., 2007, MNRAS, 376, 1480
- Oh S.-H., de Blok W.J.G., Brinks E., et al., 2011, AJ, 141, 193
- Ostlin G., Amram P., Masegosa J., et al., 1999, A&AS, 137, 419
- Ott J., Stilp A.M., Warren S.R., et al., 2012, AJ, 144, 123
- Rhee M.-H., & van Albada T.S., 1996, A&AS, 115, 407
- Simpson C.E., Hunter D.A., Nordgren T.E., et al., 2011, AJ, 142, 82
- Staveley-Smith L., Davies R.D., & Kinman T.D., 1992, MNRAS, 258, 334
- Stil J.M., & Israel F.P., 2002, A&A, 389, 42
- Swaters R.A., Sancisi R., van Albada T.S., van der Hulst J.M., 2009, A&A, 493, 871
- van Zee L., Maddalena R.J., Haynes M.P., et al., 1997, AJ, 113, 1638
- van Zee L., 2000, AJ, 119, 2757
- Young L.M., van Zee L., Lo K.Y., et al., 2003, ApJ, 592, 111
- Zasov A.V., Khoperskov A.V., 2003, Astronomy Letters, 29, 437